"CRYSTALLINE" MYOSIN CROSS-BRIDGE ARRAY IN RELAXED BONY FISH MUSCLE

Low-Angle X-ray Diffraction from Plaice Fin Muscle and Its Interpretation

JEFFREY HARFORD AND JOHN SQUIRE
Biophysics Section, Blackett Laboratory, Imperial College, London SW7, England

SUMMARY Detailed structural analysis of muscles normally used to study myosin cross-bridge behavior (e.g., frog sartorius muscle, insect flight muscle) is extremely difficult due to the statistical disorder inherent in their myosin filament arrays. Bony fish muscle is different from all other muscle types in having a myosin filament (A-Band) array with good three-dimensional (crystalline) regularity that is coherent right across each myofibril. Rigorous structure analysis is feasible with fish muscle. We show that low-angle x-ray diffraction patterns from plaice fin muscle contain characteristic vertebrate layer lines at orders of 429 (±0.2)Å, that these layer lines are well sampled by row-lines from a simple hexagonal lattice of *a*-spacing 470 (±2.0)Å at rest length and that there are meridional reflections, due to axial perturbations of the basic helix of myosin heads, similar in position to those from frog muscle but differing in relative intensities. Clear trends based on modeling to a resolution of 130 Å of the observed intensities in the low angle x-ray diffraction pattern from relaxed plaice fin muscle suggest that: (*a*) the pattern out to 130 Å is more sensitive to the distribution of the two heads than it is to details of the head shape, (*b*) both heads in one myosin molecule probably tilt axially in the same direction by ~20–40° relative to a normal to the thick filament backbone, (*c*) the center of mass of the heads is at 145 to 160 Å radius, and (*d*) the two heads form a compact structure by lying closely adjacent to each other and almost parallel. Little rotational disorder of the heads can occur. Because of its crystallinity, bony fish muscle provides a uniquely useful structural probe of myosin cross-bridge behavior in other muscle states such as rigor and active contraction.

INTRODUCTION

X-ray diffraction studies of muscle have enormous potential as a means of probing the molecular events occurring during the contractile cycle. This is especially evident in the recent time-resolved x-ray diffraction studies of muscle where intensity changes can be followed on a millisecond time scale (Huxley et al., 1981, 1982, 1984). However a major obstacle in this work lies in the difficulty in interpreting unambiguously the observed x-ray diffraction patterns even from a static "relaxed" muscle. This problem is compounded in the case of patterns both from frog sartorius muscle and insect flight muscle since in both cases it has been found that the myosin filament arrangement is not regular but contains in-built statistical disorder (Luther and Squire, 1980; Freundlich and Squire, 1983). The statistical nature of the filament lattice in these and other higher vertebrate muscles (Luther and Squire, 1980; Fig. 1 *b*) means that the myosin layer lines in their observed x-ray diffraction patterns will each be an unknown mixture of unsampled and partially sampled intensity distributions. Extracting usable unambiguous intensity values from these layer lines to carry out satisfactory modeling is far from simple. (This problem is discussed in detail in Squire, 1981). We show here that the same problem does not apply to the muscles of bony fish where the myosin filament arrangement is regular in three-dimensions; it is virtually crystalline.

The nature of the frog A-band superlattice has been demonstrated by electron microscopy of the thick filament lattice in the bare region of the A-band (Luther and Squire, 1980) and it is consistent with the relatively complicated sampling of the myosin layer lines (from the myosin cross-bridges) in the x-ray diffraction pattern of resting frog sartorius muscle (Squire, 1981; Fig. 1 *a*). Thus it appears that in the cross-bridge region the same statistical superlattice exists; myosin thick filaments have one of two different orientations 180° apart, as shown in Fig. 1 *b*, and there is statistical disorder built into the lattice. On the other hand similar electron microscope observations of the bare-zones of bony fish muscles have shown the presence of a much simpler A-band lattice (Pepe, 1971; Luther and Squire, 1980). Since there is correlation in the case of frog sartorius muscle between the bare region superlattice and the sampling of the myosin layer lines from the cross-bridges, it is reasonable to expect that the cross-bridge lattice in fish muscle will also reflect the simple lattice observed in the bare region. If this is true then the low-angle myosin layer lines should be sampled by row-

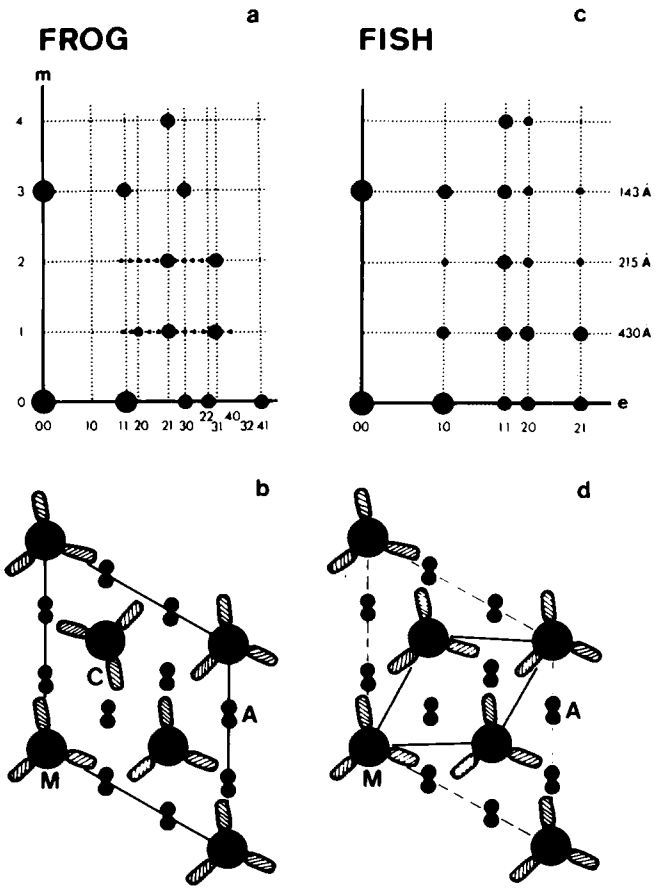

FIGURE 1 (*a*) Summary of detailed sampling of the myosin layer lines (430 Å, 215 Å, 143 Å and 108 Å) in one quadrant of the low-angle diffraction pattern from frog sartorius muscle as observed by Huxley and Brown (1967). The strongest reflections on layer lines 1, 2, and 4 are on different row lines from the strongest reflections on the equator *e* and on the third layer line at 143 Å. (*b*) Diagram of the superlattice unit cell (unbroken line) of thick filaments *M* and thin filaments *A* which has been shown to be statistically disordered. Note that the cross-bridge helices *C* on each of the thick filaments assume two different orientations. (*c*) The sampling of the myosin layer lines that would result from there being a single orientation of the thick filaments in the double hexagonal lattice as shown in *d*. Reflections appear on the same positions on all the layer lines and are only absent when the transform from the single myosin filament is zero. A simpler unit cell (unbroken line in *d*) is thus formed in the case of fish.

lines indexing on the simple hexagonal unit cell (Fig. 1 *c*); the rotational relationship between neighboring thick filaments will approximate to that shown in Fig. 1 *d*.

The low-angle x-ray diffraction studies of live bony fish muscle presented here show that the sampling of the myosin layer lines is precisely as expected from such a simple lattice of cross-bridges. These studies also show that, despite having very similar longitudinal periodicities to those of the thick filaments in frog sartorius muscle, in fish muscle there are small differences in the average cross-bridge repeat, in the axial perturbations of the cross-bridges from this average value and in the interfilament spacings at rest length. Although attempts have been made in the past to model the low-angle diffraction data from frog muscle (Squire, 1975; Haselgrove, 1980; Squire, 1981), the presence of superlattice sampling meant that the modeling could not be considered satisfactory. On the other hand, the presence of the simple row-line sampling in the diffraction pattern from fish muscle allows much more satisfactory modeling of the resting cross-bridge arrangement in a vertebrate muscle to be carried out.

We describe for the first time the low-angle diffraction pattern from a bony fish muscle; we compare the observed patterns with those from other vertebrate muscles and we model to 130 Å resolution the distribution of diffracted intensity on the layer lines due to the distribution of myosin heads in the A-band lattice. Reasonable agreement has been obtained between the calculated and the observed intensities in most of the low angle region of the myosin layer lines.

MATERIALS AND METHODS

Whole fin muscles from the ventral or dorsal fins of the plaice (*Pleuronectes platessa*) were used for the x-ray diffraction studies. During the x-ray exposure the muscle, held at its rest sarcomere length of ~2.4 μm, was bathed in aerated plaice Ringer's solution (Cobb et al., 1973) at 4°C. X-ray diagrams were recorded using cameras with the conventional mirror-monochromator design (Huxley and Brown, 1967). This incorporated focusing by a quartz crystal monochromator and a single glass mirror reflector. With an Elliott GX18 rotating anode source of x-rays operated at 40 kV, 60 mA and a distance between the specimen and film of 30 cm, the low-angle x-ray pattern was recorded within 24 h of the dissection of the muscle. Longer cameras (80 cm specimen to film distance) were used to study the very low angle pattern and for calibration purposes. X-ray diffraction patterns were recorded on CEA Reflex 25 film and measurements of the intensity distributions from them were made using a Joyce-Loebl double-beam microdensitometer (model IIIC). Measurements of the areas under the peaks in the microdensitometer traces were corrected by a simple Lorentz factor (proportional to the reciprocal lattice radius of the x-ray reflection from the meridan), and also by a multiplicity factor, to give the set of observed x-ray intensities.

Layer line intensities were computed from the equation

$$\langle I(R,1/c)\rangle_\psi = \sum_n \sum_j (A^2_{n,1} + B^2 n,1),$$

where

$$A_{n,1}(R) = \sum_j f_j J_n(2\pi R r_j) \cos [2\pi l z_j/c - \phi_j n]$$

$$B_{n,1}(R) = \sum_j f_j J_n(2\pi R r_j) \sin [2\pi l z_j/c - \phi_j n]$$

using contributions from J_0 and J_9 Bessel orders on the third layer line, J_3 and J_{-6} on the first layer line, and J_{-3} and J_6 on the second layer line. When investigating the effect of the rotation of the myosin filament within the unit cell the sampled myosin filament transform was given by

$$F(R_{hk},\psi_{hk},1/c) = \sum_n \sum_j f_j J_n (2\pi R_{hk} r_j) \exp\left[i\left\{n\left(\psi_{hk} + \frac{\pi}{2} - \phi_j\right) + 2\pi l z_j/c\right\}\right],$$

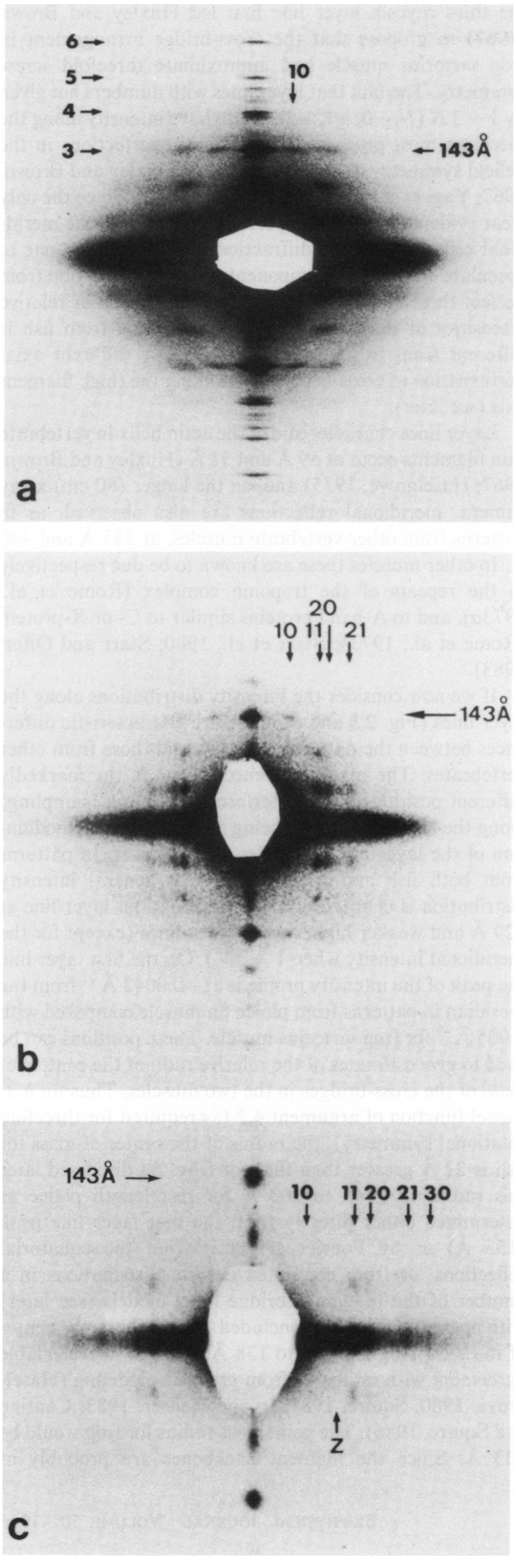

FIGURE 2 X-ray diffraction patterns of live plaice fin muscle at rest sarcomere length (2.4 μm) taken on a camera with a 30 cm specimen to film distance. The muscle fiber axis is vertical, the crystal focusing direction giving the narrow dimension of the focused x-ray beam is vertical in *a* but across the page in *b* and *c*. Vertical arrows indicate row lines and their *h*, *k* indices according to the hexagonal lattice of thick filaments of *a*-spacing 472 Å. Horizontal arrows indicate the higher order myosin layer lines which index on a repat of 429 Å. (*a*) 24 h exposure time, 40 kV 50 mA. The meridional reflections numbered 3, 4, 5, and 6 index on a repeat of 429 Å. (*b*) and (*c*) 13 h exposure time, 30 kV 50 mA. (*c*) The equatorial diffraction pattern is shown at a larger magnification. The equatorial reflection denoted *z* is most probably due to the *z*-line structure.

where

$$R_{hk} = (1/a)\sqrt{\{(4/3)[h^2 + k^2 + hk]\}}$$

$$\psi_{hk} = \tan^{-1}\left\{\frac{h + 2k}{h\sqrt{3}}\right\},$$

where the terms have their usual meaning (Franklin and Klug, 1955; Klug et al., 1958).

X-RAY DIFFRACTION FROM FISH MUSCLE

The strongest x-ray reflections in the low-angle x-ray pattern from live fish muscle occur along the equator of the pattern and arise from the hexagonal arrangement of thick and thin filaments. The spacings of these reflections index as the 10, 11, 20, 21, and 30 reflections from a hexagonal unit cell of *a*-spacing 472 Å at rest sarcomere length. This is significantly larger than the rest length *a*-spacing of 410 Å in frog muscle. As in the case of patterns from frog muscle (Huxley and Brown, 1967), the off-equatorial pattern is dominated by a series of layer lines, some with strong meridional components (Fig. 2 *a*). The spacings of these layer lines (Table I) index on a repeat of 429 Å, which is three times that of the strongest meridional reflection, that on the third layer line. This latter reflection, 143.2 Å corresponds to a spacing only 0.2 Å less than the corresponding meridional reflection in the x-ray pattern from frog sartorius muscle; a spacing taken to be 143.4 Å (Haselgrove, 1975). Relative values for both spacings were obtained using the same camera, which had an 80 cm specimen-to-film distance. This particular reflection represents the "average" axial repeat of the myosin cross-bridge levels along the thick filament; a repeat that is clearly very similar in both fish and frog muscle.

The very strong intensity of the meridional reflection on the third myosin layer line first led Huxley and Brown (1967) to propose that the cross-bridge arrangement in frog sartorius muscle had approximate threefold screw symmetry. The fact that layer lines with numbers not given by $l = 3N$ ($N = 0, \pm 1, \pm 2 \ldots$) also have intensity along the meridian most probably arises from imperfections in the helical symmetry of the cross-bridges (Huxley and Brown, 1967; Yagi et al., 1981; Squire et al., 1982). Since the only clear evidence for these imperfections is that of the meridional reflections, x-ray diffraction data only allow one to speculate on the axial component of this perturbation from perfect threefold screw symmetry. The pattern of relative intensities of these "forbidden" meridionals from fish is different from frog, suggesting a slightly different axial perturbation of cross-bridge levels along the thick filament axis (see later).

TABLE I

MYOSIN LAYER LINE SPACINGS FROM LIVE PLAICE FIN MUSCLE AT REST LENGTH

Measured spacing	Order of 429 Å	Theoretical spacing of order of 429 Å
Å		
420.5*	1	429.0
215.6*	2	214.5
143.2**	3	143.0
106.1	4	107.2
85.7	5	85.8
71.5	6	71.5
61.5	7	61.3
53.5	8	53.6
48.0	9	47.7
38.9	11	39.0

Layer line spacings were measured along the meridian except where indicated with an asterisk (*). Standard deviations of 0.2 Å or less apply to all measurements made along the meridian and standard deviations of 1 to 2 Å apply to measurements made off the meridian (*). The double asterisk (**) indicates a reflection used for calibration. Average data from 13 muscle preparations.

Layer lines characteristic of the actin helix in vertebrate thin filaments occur at 59 Å and 51 Å (Huxley and Brown, 1967; Haselgrove, 1975) and, on the longer (80 cm) x-ray camera, meridional reflections are also observed, as in patterns from other vertebrate muscles, at 385 Å and 440 Å. In other muscles these are known to be due respectively to the repeats of the troponin complex (Rome et al., 1973*a*), and to A-band proteins similar to C- or X-protein (Rome et al., 1973*b*; Starr et al., 1980; Starr and Offer, 1983).

If we now consider the intensity distributions along the layer lines (Fig. 2 *b* and *c*), there are characteristic differences between the patterns from fish and those from other vertebrates. The main differences occur in the markedly different positions of the interference maxima (sampling) along the layer lines; there being a similar overall modulation of the layer line intensities in both cases. In patterns from both fish and frog muscles the general intensity distribution is characterized by a strong first layer line at 429 Å and weaker higher order layer lines (except for the meridional intensity when $l = 3N$.). On the first layer line the peak of the intensity profile is at ~0.0043 $Å^{-1}$ from the meridian in patterns from plaice fin muscle compared with 0.005 $Å^{-1}$ for frog sartorius muscle. These positions can be used to give estimates of the relative radii of the centers of mass of the cross-bridges in the two muscles. Thus for a J_3 Bessel function of argument 4.2 (as required for threefold rotational symmetry), the radius of the center of mass for fish is 22 Å greater than that for frog. As discussed later this radius is ~145 to 160 Å for rest length plaice as determined either directly from the first layer line peak (155 Å) or by Fourier synthesis from the equatorial reflections, or from computed density distributions in a number of the best cross-bridge helix models (see later) with no myosin backbone included. On this basis the center of mass for frog is ~123 to 138 Å; a range in reasonable agreement with estimates from previous modeling (Haselgrove, 1980; Squire, 1981; Ip and Heuser, 1983; Cantino and Squire, 1986). The point mass radius for frog would be 133 Å. Since the filament backbones are probably of

similar diameters in both muscles (Luther and Squire, 1980; Luther et al., 1981) this means that the cross-bridges have their centers of gravity at a greater radius from the thick filament surface in fish muscle; this would fit in well with the larger lattice spacing and interfilament spacing in the case of fish. The distance between the thick and thin filament axes is ~270 Å in rest length plaice muscle compared with 240 Å for frog sartorius muscle (Huxley, 1968).

LATTICE SAMPLING OF THE FISH LAYER LINE PATTERN

In x-ray diffraction patterns from plaice fin muscles, the layer line intensity is only observed at certain well-defined sampling positions. On the equator (Fig. 2 *c*) the first few diffraction peaks index as the 10, 11, 20, 21, and 30 reflections from a simple hexagonal unit cell (Fig. 1 *d*; Table II). Unlike the relatively complicated patterns from frog muscles (Fig. 1 *a*), diffraction peaks on all of the other myosin layer lines from fish muscle only occur on the same row-lines as those reflections which appear on the equator (Figs. 2 *b* and *c*) and there is no significant unsampled intensity between these peaks. This simple sampling pattern, which has so far been seen up to at least the sixth myosin layer line (at 72 Å) is completely consistent with the cross-bridges in fish muscle forming a simple unit cell (Fig. 1 *d*) identical in shape and size to that deduced from the equatorial pattern. The breadth of these row-line peaks along the layer lines also suggests that the order of the cross-bridge lattice is as extensive as the myofibril width. Thus myosin cross-bridge helices on neighboring thick filaments within each myofibril must be in good rotational and axial register, and must be located on a well-defined three-dimensional lattice; the cross-bridge array within each A-band is essentially "crystalline". The clear correlations between the bare zone lattices and the cross-bridge arrays in both fish and frog muscles show that, as expected, myosin filaments behave as relatively rigid assemblies in which the orientation of the cross-bridge arrays is defined by the azimuthal orientation of the filaments in the M-band (Luther et al., 1981).

TABLE II

ROW LINE SPACINGS FROM "TWO-DIMENSIONALLY RESOLVED" X-RAY DIFFRACTION PATTERNS AND THEIR INDEXING ON THE A-BAND HEXAGONAL LATTICE AND I-BAND SQUARE LATTICE

Index on 290 Å square lattice	Index on 472 Å cell hexagonal lattice	Calculated spacing	Observed spacing
—	10	408.8	409.1
10	—	290.0	290.0
—	11	236.0	233.6
11	20	204.4	204.4*
—	21	154.5	153.7
—	30	136.3	134.1

Lattice spacings were measured along the equator of the diffraction pattern from plaice fin muscle. Hexagonal unit cell size is 472 Å determined from the 204.4 Å *20* equatorial reflection. Probable error on the measurement of spacings is 0.5%. The corresponding five row line reflections along the first layer line occurred within 0.2% of the spacing measured along the equator, as did the *10* and *11* reflections along the third and second layer lines, respectively.

*Note that the *11* reflection from the I-band coincides with the *20* reflection from the A-band. This should be considered in modeling equatorial diffraction data from vertebrate muscle.

MODELING THE OBSERVED INTENSITY DISTRIBUTIONS TO 130 Å RESOLUTION

Although x-ray intensities on the myosin layer lines from bony fish muscle are now being collected out to a resolution of 70 Å, we chose to carry out the initial modeling reported here to a resolution of only 130 Å. The main reason for this was that at this resolution the precise details of the shape of the myosin head (i.e., head curvature) are not crucial provided that the maximum chord length and mass distribution are approximately correct; slight alterations of diameter of the heads or their curvature would have relatively minor effects. Even excluding this feature the initial modeling to 130 Å required the computation of the transforms of 30,000 different myosin head arrangements. The introduction of head curvature, as shown in recent electron micrographs (Walker et al., 1985; Rayment and Winkelmann, 1984; Winkelmann et al., 1985) and as required for modeling the x-ray diffraction data at higher resolution, would have increased the number of combinations of model parameters, due to the unknown orientation of each head around its own long axis, by a factor of at least 144 times (allowing 30° increments of orientation). It is well known that such details would only have a marked effect on the relatively high angle region of the Fourier transform of a single myosin head. On the other hand the relative disposition of the two heads on each lattice site is bound to have a very marked effect on the calculated transform as our modeling has shown. The separation of the outer ends of the two heads could in theory be anything between 50 Å and 300–400 Å and the spacing range 130–500Å is the one being modeled.

In summary the region that we are modeling is sensitive above all other things to the relative positions of the two heads on each lattice site and, provided the chosen head model has approximately the correct shape, the modeling results will be valid. When all the higher resolution data are collected and when the head shape is more accurately defined from studies of S-1 crystals (Winkelmann et al., 1985) further modeling will be carried out to 70 Å resolution.

DEFINING A SUITABLE MODEL

(*a*) For reasons given above our low resolution model defined each myosin head as being a figure of rotation similar to that used by Offer et al. (1981) and based on the micrograph data of Elliott and Offer (1978). Each head

was modeled either as a set of nine overlapping spheres (Table III) generating a diffracting unit of maximum chord length ~190 Å (long head) or slightly shorter by the omission of the inner two spheres from the long head model (short head - maximum chord ~160 Å). For comparison Elliott and Offer put the maximum chord length at 180 to 200 Å and Winkelmann et al. (1985), although estimating the length along the curved head to be >160 Å (i.e., between 160 Å and 200 Å), describe heads where the maximum chord length appears to be only ~130 to 160 Å.

(*b*) The myosin filament helix was taken to be three-stranded (Squire, 1972) based on the known threefold symmetry of fish myosin filaments (Luther et al., 1981) and the known three-stranded structure of other vertebrate thick filaments (Ip and Heuser, 1983; Kensler and Stewart, 1983; Cantino and and Squire, 1986). The heads of one mysoin molecule were taken to be located on each lattice point (Tregear and Squire, 1973; Reedy et al., 1981).

(*c*) The axial perturbation of the cross-bridge array was taken to be minor enough to be ignored during initial low resolution modeling. The presence of the perturbation is indicated by the existence of "forbidden" meridional reflections at orders of the 429 Å repeat other than $1 = 3N$. One-dimensional modeling (Squire et al., 1982) shows that the condition in fish x-ray patterns where the fourth order is stronger than the fifth and where the second order is weak, arises from a cross-bridge array where in the 429 Å repeat successive cross-bridge levels are separated not by equal 143 Å intervals but by ~160 Å, 140 Å, and 130 Å. This is less of a distortion than that in frog where the relatively strong second and fifth orders require intervals of ~155 Å, 115 Å, and 155 Å. Later modeling of fish myosin filaments to 70 Å will include this feature; it may account for some of the features unexplained by the modeling results described below.

MODEL PARAMETERS AND THE ASSESSMENT OF GOODNESS OF FIT

Visualization of myosin molecules by electron microscopy (Elliott and Offer, 1978) and indirect measurements of their flexibility (Mendelson et al., 1973; Thomas et al., 1975) suggest that in isolated molecules the heads can have considerable freedom of movement about the junction where they are joined to the tail of the myosin molecule. The positions of the two heads were therefore independently incremented (by 30° intervals) through a tilt, β (Fig. 3 *a*), measured from the plane perpendicular to the thick filament axis and a slew, α (Fig. 3 *b*), measured from the normal to the thick filament surface at the point where the heads originate from the surface. α and β were both varied between ±90°. The heads were placed so that the center of the innermost sphere of each head was at a radius, R, which varied between 80 Å and 120 Å (in 10 Å intervals) for the seven-sphere head model and between 60 Å and 100 Å for the nine-sphere model. A feature was included in the computations so that sterically impossible configurations causing overlap of the two heads were automatically excluded. A further variable was included in case the origins of the two heads are not at the same axial level. The angle γ (Fig. 3) was varied to do this. It is the orientation of a line through the origins of the two heads in a plane tangential to the thick filament surface.

At each radius, R, and for each configuration of the heads defined by α_1, β_1, α_2, β_2, and γ, the intensity along the first three myosin layer lines was computed (see Methods) to ~130 Å resolution (i.e., up to the 30-row line) and was compared with the observed intensity (Table IV).

TABLE III

PARAMETERS USED TO MODEL THE MYOSIN HEAD SHAPE WITH OVERLAPPING SPHERES

Distance of center of sphere from the center of the first sphere in Angstrom	0*	16*	32	48	64	83	107	135	163
Radius of sphere in Angstroms	11.5	11.5	11.5	11.5	12.5	16	20	23	19

*These two spheres were omitted for the short head model.

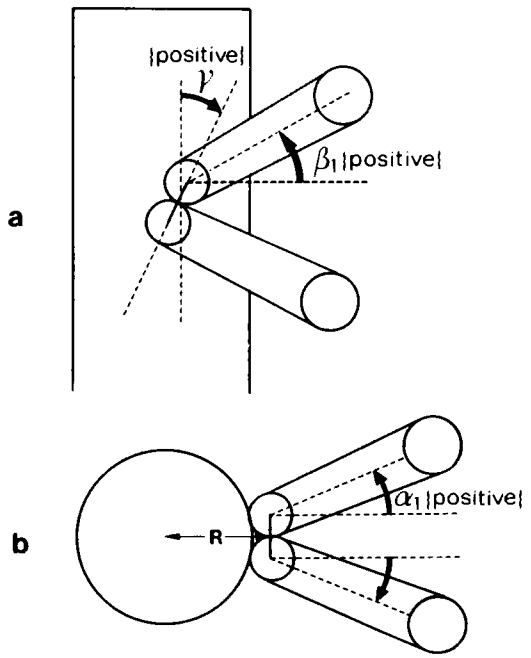

FIGURE 3 Diagram showing the angles α, β, and γ used to define the orientation of the models of the myosin heads. (*a*) γ defines the relative positions of the two head origins in a plane tangential to the thick filament surface. β, the axial tilt, refers to the angle, measured in a vertical plane (i.e., parallel to the fiber axis), of the head axis from the plane normal to the thick filament axis. (*b*) An end-on view of the cross-bridge model. The slew, α, is measured in a horizontal plane, from the normal to the plane that is tangential to the thick filament surface. The two heads have individual slews and tilts, which are denoted by subscripts 1 and 2. R is the radius of the center of the innermost sphere of each head.

TABLE IV

CORRECTED RELATIVE INTENSITIES FROM "TWO-DIMENSIONALLY RESOLVED" X-RAY PATTERNS

Layer line number	Row-line intensities				
	10	11	20	21	30
3	7	14	3	vw	vw
2	1**	18	1**	vw	vw
1	4*	43	28	10*	3*

Probable error on intensity measurements is 10 to 15%. Reflections indicated by an asterisk (*) have probable errors of 25% to 30%. These errors include measurements made with slightly different background assumptions and values from densitometer traces along row lines and layer lines. All intensities were scaled to the *11* peak on the first layer line which was assigned a value of 43 after scaling it to the *11* equatorial reflection. This latter reflection was given an arbitrary value of 200. The observed intensities have been corrected for a simple Lorentz factor by multiplying by the reciprocal of the row line spacing. The *21* row line intensities were divided by 2 to account for the multiplicity. Reflections indicated by a double asterisk (**) were just visible on films of the patterns but not measurable on microdensitometer traces of films. These were assigned a value of 1 on the basis of their intensity relative to the weakest reflections that were measurable.

The effect of changing the absolute orientation of the filament in the hexagonal lattice was found to be minor so that variations in the 21 and 30 reflections were very much smaller than the experimental error on the intensity measurements available at present for these reflections. The observed and computed intensities (I_o and I_c, respectively) were initially compared by computing the least sum of squares $R_s = \Sigma_1^n\ w_n\ (I_o - I_c)^2$ (the weighting factor used throughout was $w = 1$). Following this initial screening of >30,000 models considered, most of which gave unacceptable intensities, the remaining 100 or so models were further scrutinized using three different objective tests of "goodness of fit". One was the least sum of squares R_s defined above. The second was a conventional R-factor calculation based on observed and calculated amplitudes (F_o and F_c): $R_F = \Sigma_1^n \parallel F_o| - |F_c \parallel \Sigma_1^n |F_o|$. The third was an R-factor, based on intensities, of the form: $R_I = \Sigma_1^n I_o - I_c|/\Sigma_1^n I_o$. This third factor ($R_I$) can be considered similar to the second (R_F) except that stronger reflections now have a larger weighting. Since each type of assessment has its own advantages and disadvantages we considered them all and compared the results. When all of the short-listed models

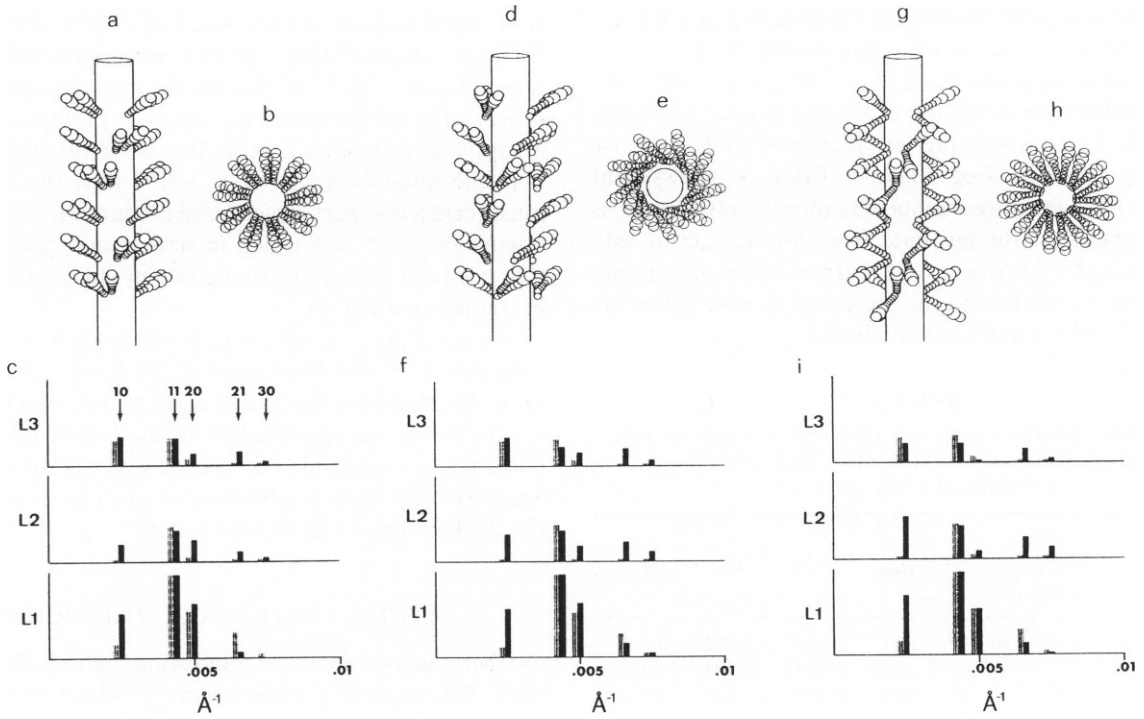

FIGURE 4 Representations of cross-bridge helix models and their computed transforms. For each configuration discussed in the text there is shown a perspective view of the cross-bridge model (*a*, *d*, and *g*), an end-on view of three cross-bridge levels (*b*, *e*, *h*) and a bar-chart plot of the observed and computed intensity on the first three myosin layer lines (L1, L2, and L3) in one quadrant of the diffraction pattern (*c*, *f*, *i*). At the five row-line positions (*h*, *k* corresponding to 10, 11, 20, 21, 30) along each layer line (indicated by vertical arrows in *c*) the observed intensity is represented by a lightly shaded bar (shown to the left of the actual observed position) and the computed intensity by a dark (filled) bar to the right. The observed intensities shown have been corrected for the Lorentz and multiplicity factors. In *a*, *d*, and *g* a cylinder representing the thick filament backbone is shown with a 70 Å radius for reference purposes only. Intensities were scaled to the strongest peak (i.e., 11 row-line) on the first layer line. To account for temperature disorder the outer sphere of each head had a root mean square isotropic displacement of 11.5 Å applied and successive spheres at lower radii were decremented from this so that the innermost sphere had zero displacement. Larger displacements have been tried as described in the text. (*a*) Seven-sphere head model with the center of the innermost sphere of each head at 77 Å radius; $\beta_1 = \beta_2 = 30°$; $\alpha_1 = 30°$, $\alpha_2 = 0°$; $\gamma = 60°$. (*d*) Nine-sphere head at 100 Å radius; $\beta_1 = \beta_2 = 30°$; $\alpha_1 = 60°$, $\alpha_2 = 90°$; $\gamma = 0°$. (*g*) Nine-sphere head model at 70 Å radius; $\beta_1 = 30°$, $\beta_2 = -30°$; $\alpha_1 = 30°$, $\alpha_2 = 0°$; $\gamma = 0°$.

were assessed with these different factors, it was found that on the whole the same models gave good fits using any of the different factors. However, because there were a number of possible models with reasonable R-factors we were keen to deduce from our analysis any important objectively assessed general trends that promote a good fit. We consider these trends below.

RELATIVELY UNAMBIGUOUS TRENDS OF THE MODELING

Having reduced the number of models down to the last 20–40 each, for either the short head or the long head versions of the cross-bridge, it became clear that, as far as head tilt (β) was concerned there were only two viable cases. In one group of models (see Fig. 4 *a*) the two heads were tilted in the same direction by ~30° ($\beta_1 = +30°, \beta_2 = +30°$) and in the other (see Fig. 4 *g*) the two heads were tilted in opposite directions by 30° ($\beta_1 = +30°, \beta_2 = -30°$). To assess the quality of fit given generally by these two types of model, we tabulated both the number of plausible models and the mean R-factor value of the best few models in each category (Table V). The results for the different R-factors and for the long- and short-head models show the clear trend that good fits are very much easier to achieve if both of the heads tilt in the same direction ($\beta_1 = \beta_2 = +30°$). The other possibility ($\beta_1 = +30°, \beta_2 = -30°$), but with a combination of smaller radius and greater slew than is possible for fish, was the one preferred by Haselgrove (1980) for relaxed frog muscle. Table V shows that although this structure cannot be entirely ruled out it is clearly not favored by our data from fish; in fact, it only gives reasonable fits over a very narrow range of parameters, whereas models with the preferred tilt give better fits (see later) and are more broadly based.

TABLE V

MEAN VALUES OF THE FIVE LOWEST R-VALUES FOR EACH TYPE OF R-FACTOR FOR THE BEST TWO COMBINATIONS OF TILT

	Tilts β_1, β_2 (degrees)	N*	R_S‡	R_I‡	R_F‡	R_F§
Seven-sphere head	+30, +30	21	314	0.474 (0.454)	0.312 (0.308)	0.316 (0.287)
	+30, −30	11	299 (283)	0.474	0.328	0.316
Nine-sphere head	+30, +30	21	293 (268)	0.468 (0.461)	0.308 (0.297)	0.314
	+30, −30	9	330	0.500	0.336	0.328 (0.281)

*N is the number of models with values of $R_S(=\Sigma_1^n |I_o - I_c|^2)$ less than 400.

‡The actual minimum values for the respective R-factors are shown in parentheses.

§This is the R-factor for amplitudes with 11.5A r.m.s isotropic displacement disorder factor applied as described in the text.

Turning now to the slews and radii of the two heads, the modeling is less clear cut. However, there is a very clear trend that good fits are either obtained with large radii (80–100 Å) and large slews (60–90°), or smaller radii (70–80 Å) and smaller slews (30–60°) and so on; a correlation needed to keep the center of mass of the heads at about the radius required by the peak of the intensity envelopes along the first and second layer lines. It was mentioned earlier that if the myosin heads are considered as point masses qiving rise to an intensity peak at 0.0043 $Å^{-1}$ on the first layer line, the masses would have a calculated radius of 155 Å. In all of the models giving relatively low R-factors the calculated mean radius of the center of mass of the two heads was almost always within the range 145–165 Å; a result in good agreement with the point mass approximation. Thus the position of the center of mass of the two heads is rather well defined by the modeling.

Another important feature concerns the relative slews of the two heads. In all of the models with $\beta_1 = \beta_2 = +30°$ it was found that α_1 and α_2 always differed by 30°. In this case, with both heads at the same tilt, their slews could not usually be equal, due to steric overlap, but the difference in slew might have been 60°, 90°, 120°, 150°, or even 180°. Without exception, in the short-listed models, it was 30°. A larger relative slew of the heads gave patterns totally different from the observed intensity profiles. Thus the analysis shows unambiguously that if the tilt of both heads is in the same direction ($\beta \sim +30°$) then the two heads must form a compact structure to account for the observed intensities; a 30° separation in slew in our models means that heads with the same tilt lie side by side and are almost in contact (see Fig. 5).

In summary, we have found trends such that (*a*) the most likely models have both of the heads tilting in the same direction; (*b*) the tilt is nearer to 30° than 0° or 60°; (*c*) the heads are separated by a small slew difference so that they are alongside each other; and (*d*) the heads are arranged with their mean center of mass at a radius from the thick filament axis of 145–160 Å.

SPECIAL FEATURES OF THE MODELING

Further analysis shows up interesting features and limitations of the present modeling, some of which will influence future modeling studies.

(*a*) Reasonable agreement with I_o could be obtained on almost all reflections except 101, 102, and 202, which were without exception modeled to be much too strong, and 211 which was always modeled too weak.

(*b*) The agreement with I_o on the second layer line was generally poorer for models with $\beta_1 = +30°, \beta_2 = -30°$ than with both heads tilting at +30°. This supports our conclusion from Table V that both heads probably tilt in the same direction.

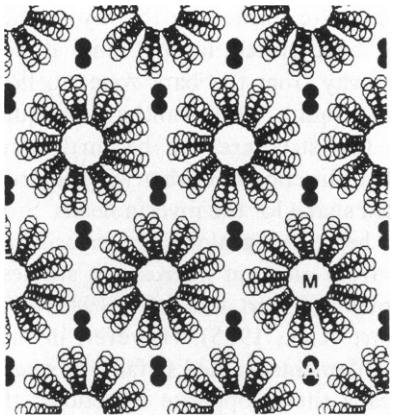

FIGURE 5 End-on view of the cross-bridge helix model shown in Fig. 4 *a*, which gives the best fit to the x-ray patterns from live plaice fin muscle, incorporated into a schematic hexagonal lattice of thick and thin filaments. The thick filament backbone is represented by an empty circle *M* and the thin filaments by two filled circles *A*. Three levels of cross-bridges are shown. The spacing between thick filaments represents the rest length lattice spacing in plaice fin muscle of 472 Å. The short model myosin heads both have 30° tilts, and are slewed by 0° and 30°. γ is equal to 60°. With this and any of the models in Table VI the heads are placed with their outer ends within 10 to 20 Å of the thin filaments.

(*c*) Some features of the low-angle pattern were relatively insensitive to the modeling. These include the third layer line, which was generally well modeled, and the reflections in (*a*), which were always poorly modeled.

(*d*) It was generally easier to obtain a reasonable fit with the short head models (maximum chord 160 Å) than the long head models (maximum chord 190 Å). This chord length in the S-1 crystals studied by Winkelmann et al. (1985) appears to lie in the range 130–160 Å. These authors quote a longer total length following the curvature of the heads (160–200 Å). In our modeling it is the maximum chord that is the important feature of the head dimensions.

(*e*) In attempting to suggest a specific most likely structure we have resisted the temptation to quote a model with the lowest *R*-value. The reason for this is that a model giving the lowest value of R_F, say, did not necessarily give the lowest R_I or R_s. However by taking into account all of the different *R*-factors and also the general shapes of the computed transforms (Table VI), we have concluded that for the long head the model with R = 60 Å, $\gamma = 0°$, $\alpha_1 = 30°$, $\alpha_2 = 0°$, $\beta_1 = \beta_2 = 30°$ ($R_F \sim 0.3$) is marginally better than a long head model with R = 100 Å, $\gamma = 0°$, $\alpha_1 = 60°$, $\alpha_2 = 90°$, $\beta_1 = \beta_2 = 30°$. However the best general fit appears to come from a short head model with R = 78 Å, γ

TABLE VI

THE PARAMETERS AND CALCULATED INTENSITIES FOR MODELS WITH BEST FITS TO THE OBSERVED INTENSITIES

Model parameters						Calculated intensities															Score‡
						ll = 3					*ll* = 2					*ll* = 1					
N§	Δu¶	*R*‖	γ	α_1	α_2	10	11	20	21	30	10	11	20	21	30	10	11	20	21	30	
7	0	76	0	30	0	5.7	13.2	6.4	6.3	4.5	3.6	15.6	13.6	11.0	13.2	9.9	43	34.4	3.7	3.4	6 + 1
7	0	86	0	30	0	5.1	10.3	4.6	6.5	3.4	5.0	16.5	13.3	14.2	14.6	13.1	43	29.2	3.7	5.4	5 + 1
7	0	87	30	30	0	6.5	12.3	5.7	8.0	4.0	5.0	15.8	11.9	10.5	10.7	13.6	43	28.1	1.9	3.6	5 + 1
7	11.5	76	0	0	−30	6.4	10.3	5.8	7.7	7.0	4.1	16.1	14.1	7.7	7.0	12.1	43	33.1	4.6	3.4	6 + 2
*7	11.5	77	30	0	−30	7.3	12.0	6.5	5.3	4.8	4.1	15.1	12.6	5.3	4.8	12.5	43	32.3	3.2	2.1	6 + 3
*7	11.5	78	60	30	0	8.8	14.9	7.8	5.9	4.3	4.9	16.5	12.5	3.7	3.6	12.6	43	31.9	2.1	0.7	6 + 3
7	11.5	83	60	60	30	7.0	13.5	7.2	5.2	3.6	4.2	13.6	10.2	4.1	4.7	12.1	43	32.8	2.1	0.3	5 + 3
9	0	60	0	30	0	9.5	12.0	4.6	7.1	4.2	4.7	15.4	12.5	14.7	15.6	12.7	43	30.1	4.0	4.3	5 + 1
9	11.5	100	0	60	90	8.6	10.2	7.7	7.4	4.5	7.6	15.8	8.9	7.2	8.3	14.2	43	31.5	5.3	2.8	5 + 1
Observed intensities						7	14	3	vw	vw	1	18	1	vw	vw	4	43	28	10	3	
Acceptable ranges for a reflection to score						≤10	≥10 ≤I_{112}**	≤8	≤5	≤5	≤5	≥15	—	≤5	≤5	—	—	≤35 ≥26	≥I_{301}**		

For all of the models shown the tilts (β_1 and β_2) are equal to 30° (see text for details).

*Preferred models.

‡The first number is the score for the strong reflections 103, 113, 203, 102, 112, 201. The second number is the score for the weak outer reflections 213, 303, 212, 302. However the latter peaks should be more sensitive to precise details of the head shape. The reflections not included in the scoring are relatively insensitive to the model parameters.

§*N* = Number of spheres in the cross-bridge model head.

‖*R* = Radius of the center of the innermost sphere of each head. Although this was incremented by values of 10Å, for the seven-sphere models this radius also depends on the other model parameters.

¶Δu = the root mean square isotropic displacement for the outermost sphere of each head (see text for details). The observed intensities shown are the peak areas from densitometer traces of the x-ray films, corrected for a simple Lorentz factor and for multiplicity and then scaled to the *11* reflection of the first layer line.

**In these cases the ratio of the intensities between certain strong reflections was considered an important selection criterion.

$= 60°, \alpha_1 = 30°, \alpha_2 = 0°, \beta_1 = \beta_2 = 30°$, and a small amount of thermal disorder (see below).

EFFECTS OF DISORDER

The fit to the observed data cannot be significantly improved by giving the heads a large amount of rotational (thermal) disorder. In an attempt to define the possible effects of disorder on the cross-bridge array, radially increasing isotropic temperature factors were applied to each of the spheres constituting each head. The sphere at the inner end of the head was given zero root mean square isotropic displacement, Δu, and subsequent spheres had Δu incremented by a constant value δ so that the nth sphere had a displacement of $n \times \delta$. This therefore modeled a head tethered at the filament surface but free both to swing and to undergo internal molecular motions and is probably more realistic than a factor related to rotational movement alone. The fit for the preferred models was marginally improved for Δu equal to 11.5 Å (Table VI). However, in the whole range of configurations modeled an increase in Δu above ~11.5 Å was accompanied by a significantly poorer fit especially in the short head models. Values of Δu of 11.5 Å, 23 Å, and 50 Å for the outer sphere were tested, but if Δu was >11.5 Å the calculated intensity distributions were totally unacceptable. Thus large disorders of the type suggested by EPR studies of probes attached to cross-bridges in skinned or glycerinated rabbit muscle fibers (Thomas et al., 1980; Thomas and Cooke, 1980), have been unable to account for the observed relative layer line intensities for fish muscle in any of the modeling carried out so far. With Δu equal to 50 Å, the global reliability factors, R_F, of the best models were very large (~0.4) and the computed intensity distributions were clearly very unsatisfactory. An alternative type of disorder in which the heads are not tethered at the filament surface, but can rotate freely in space would agree with results from Poulsen and Lowy (1983) and Thomas et al. (1980) but there is no obvious reason in this case why any layer line intensity at all would be retained; there would be nothing constraining the heads to lie on a helix.

Table V shows that the conclusion that both heads tilt in the same direction is not greatly affected by the introduction of limited thermal disorder (Δu = 11.5 Å). Although the best R-factor for the long head model was better for tilts of $+30°$ and $-30°$ none of the long head models in this case gave a fit that could be considered at all satisfactory on the first and second layer lines. Some of the short head models gave a very good fit and here the 30°, 30° configuration is clearly favored.

IMPLICATIONS ABOUT FUTURE STRUCTURAL STUDIES OF THE CONTRACTILE MECHANISM IN MUSCLE

The resting cross-bridge configuration in plaice fin muscle supports the idea that the long-pitched helical strands of density observed in electron micrographs of vertebrate thick filaments are formed by the myosin heads in each cross-bridge being tilted in the same direction (either towards or away from the bare zone) to lie along these helical tracks (Squire, 1981; Cantino and Squire, 1986). In the future, this structure can be further refined using higher angle diffraction data that will require the use of a more detailed shape for the myosin heads. Similar conclusions about heads lying along the myosin helical tracks have come from electron microscopy studies of isolated myosin filaments (Vibert and Craig, 1983; Crowther et al., 1985; Stewart et al., 1985). However, in the case of all invertebrate filaments studied so far it has been concluded that the heads tilt in opposite directions; the preferred structure is different from our preference for fish muscle. Whether this is a genuine difference between vertebrate and invertebrate thick filaments remains to be seen. However, it should be remembered that in three-dimensional reconstructions from electron micrographs as well as in the present x-ray diffraction modeling, choosing between the two classes of structure is not easy.

Fig. 5 shows that the preferred cross-bridge helix model for plaice shown in Fig. 4 *a* puts the myosin heads close to the thin filament surface (i.e., within 10 or 20 Å). This is true of all of the short listed models in Table VI, although different degrees of slew or tilt would be required in these various models for the heads to make contact with the thin filaments. However such angles cannot be determined without knowing the azimuthal rotation of the cross-bridge helix relative to the unit cell. It is possible to determine this rotation only in the case of a crystalline specimen such as fish muscle. Here, it requires very accurate data not only for the 21 and 30 row-lines but for other row-lines at higher radii since it is at these large radial positions in the myosin filament transform that significant overlap of Bessel functions occurs to give any azimuthal variation in the intensity. Layer line sampling has now been observed to a resolution of ~70 Å, which means that not only will it be possible to define more completely the configuration of the heads in relaxed muscle but, with the thick filament orientation also defined, it will be possible to consider very specifically the movements needed for these heads to interact with the neighboring thin filaments in the lattice.

Our x-ray diffraction analysis of fish muscle has shown very clearly that a simple myosin cross-bridge lattice exists in fish and is regular and well-ordered throughout each myofibril. There is very little trace of "unsampled" layer line streaks between the observed Bragg reflections. Thus it is not possible in the case of fish muscle that the heads all have total orientational disorder as suggested by probe studies of other muscles (Thomas et al., 1980; Thomas and Cooke, 1980).

The crystallinity in fish muscle not only aids x-ray diffraction work but it has also enabled considerable advances in electron microscopic analysis of the region of the muscle A-band where myosin cross-bridges are not present (Luther, 1978; Luther and Squire, 1978, 1980;

Squire, 1981; Luther et al., 1981; Luther and Crowther, 1984; Crowther and Luther, 1984). But of most significance is that bony fish muscle, with its crystalline structure, should prove to be a uniquely useful tool for studying cross-bridge behavior. We believe it should be possible in this case to relate changes that we have now observed in time-resolved x-ray diffraction studies of active fish muscle to a known starting structure; rigorous testing of the swinging cross-bridge model should then be more easily achieved.

Finally, the fact that the A-band in bony fish muscle is totally different from all other vertebrate A-bands not only demonstrates that there are two distinct classes of vertebrate skeletal muscle, but it also poses very interesting questions about vertebrate muscle evolution. The evolutionary story is especially interesting since preliminary data on the muscles of cartilaginous fish and even of the body muscle of the primitive chordate *Amphioxus* show that their A-band structures are more like higher vertebrate A-bands than like bony fish (Squire, J. M., M. Leclerc, P. K. Luther, M. Chew, A. Freundlich, and J. J. Harford, unpublished data). It remains to be seen what functional differences these two different cross-bridge arrangements have.

We are indebted to Prof. R. M. Simmons and Dr. M. Spencer for provision of x-ray diffraction facilities used in the early part of this work at the Biophysics Department, Kings College, London. We also thank Fred Huggins, Tom Rutherford, Ian Coole and Glenn Wallington for technical support, and Drs. Pradeep Luther and Alan Freundlich for many helpful discussions.

We are pleased to acknowledge support from the Muscular Dystrophy Association of America and the British Medical Research Council.

Received for publication 16 August 1985 and in final form 22 November 1985.

REFERENCES

Cantino, M. E., and J. M. Squire. 1986. *J. Cell Biol.* 102:610–618.

Cobb, J. L. S., N. C. Fox, and R. M. Santer. 1973. *J. Fish Biol.* 5:587–591.

Crowther, R. A., and P. K. Luther. 1984. *Nature (Lond.)*. 307:569–570.

Crowther, R. A., R. Padron, and R. Craig. 1985. *J. Mol. Biol.* 184:429–440.

Elliott, A., and G. Offer. 1978. *J. Mol. Biol.* 123:505–519.

Franklin, R. E., and A. Klug. 1955. *Acta Cryst.* 8:777–780.

Freundlich, A., and J. M. Squire. 1983. *J. Mol. Biol.* 169:439–453.

Haselgrove, J. C. 1975. *J. Mol. Biol.* 92:113–143.

Haselgrove, J. C. 1980. *J. Mus. Res. Cell Motil.* 1:177–191.

Huxley, H. E. 1968. *J. Mol. Biol.* 37:507–520.

Huxley, H. E., and W. Brown. 1967. *J. Mol. Biol.* 30:383–434.

Huxley, H. E., A. R. Faruqi, M. Kress, J. Bordas, and M. H. J. Koch. 1982. *J. Mol. Biol.* 158:637–684.

Huxley, H. E., M. Kress, A. R. Faruqi, M. H. J. Koch, and J. Hendrix. 1984. 8th International Biophysics Congress. Bristol. 103.

Huxley, H. E., R. M. Simmons, A. R. Faruqi, M. Kress, J. Bordas, and M. H. J. Koch. 1981. *Proc. Natl. Acad. Sci.* 78:2297–2301.

Ip, W., and J. Heuser. 1983. *J. Mol. Biol.* 171:105–109.

Kensler, R. W., and M. Stewart. 1983. *J. Cell Biol.* 96:1797–1802.

Klug, A., F. H. C. Crick, and H. W. Wyckoff. 1958. *Acta. Cryst.* 11:199–213.

Luther, P. K. 1978. Ph.D. thesis. London University. 208 pp.

Luther, P. K., and R. A. Crowther. 1984. *Nature (Lond.)*. 307:566–568.

Luther, P. K., P. M. G. Munro, and J. M. Squire. 1981. *J. Mol. Biol.* 151:703–730.

Luther, P. K., and J. M. Squire. 1978. *J. Mol. Biol.* 125:313–324.

Luther, P. K., and J. M. Squire. 1980. *J. Mol. Biol.* 141:409–439.

Mendelson, R. A., M. F. Morales, and J. Botts. 1973. *Biochemistry.* 12:2250–2255.

Offer, G., J. Couch, E. J. O'Brien, and A. Elliott. 1981. *J. Mol. Biol.* 151:663–702.

Pepe, F. A. 1971. *Prog. Biophys.* 19:75–96.

Poulsen, F. R., and J. Lowy. 1983. *Nature (Lond.)*. 303:146–152.

Rayment, I., and D. A. Winkelmann. 1984. *Proc. Natl. Acad. Sci.* 81:4378–4380.

Reedy, M. K., K. R. Leonard, R. Freeman, and T. Arad. 1981. *J. Mus. Res. Cell Motil.* 2:45–64.

Rome, E. J., T. Hirabayashi, and S. V. Perry. 1973*a*. *Nature (Lond.)*. 244:154–155.

Rome, E. J., G. Offer, and F. A. Pepe. 1973*b*. *Nature (Lond.)* 244:152–154.

Squire, J. M. 1972. *J. Mol. Biol.* 72:125–138.

Squire, J. M. 1975. *Annu. Rev. Biophys. Bioeng.* 4:137–163.

Squire, J. M. 1981. The Structural Basis of Muscular Contraction. Plenum Publishing Corp., New York. 698 pp.

Squire, J. M., J. J. Harford, A. C. Edman, and M. Sjostrom. 1982. *J. Mol. Biol.* 155:467–494.

Starr, R., P. M. Bennett, and G. Offer. 1980. *J. Mus. Res. Cell Motil.* 1:205–206.

Starr, R., and G. Offer. 1983. *J. Mol. Biol.* 170:675–698.

Stewart, M., R. W. Kensler, and J. C. Levine. 1985. *J. Cell Biol.* 101:402–411.

Thomas, D. D., and R. Cooke. 1980. *Biophys. J.* 32:891–906.

Thomas, D. D., S' I. Ishiwata, J. C. Seidel, and J. Gergely. 1980. *Biophys. J.* 32:873–890.

Thomas, D. D., J. C. Seidel, J. S. Hyde, and J. Gergely. 1975. *Proc. Natl. Acad. Sci. USA.* 72:1729–1733.

Tregear, R. T., and J. M. Squire. 1973. *J. Mol. Biol.* 77:279–290.

Vibert, P., and R. Craig. 1983. *J. Mol. Biol.* 165:303–320.

Walker, M., P. Knight, and J. Trinick. 1985. *J. Mol. Biol.* 184:535–542.

Winkelman, D. A., H. Mekeel, and I. Rayment. 1985. *J. Mol. Biol.* 181:487–501.

Yagi, N., E. J. O'Brien, and I. Matsubara. 1981. *Biophys. J.* 33:121–138.